PHYSICAL REVIEW D **78,** 063542 (2008)

Conservative constraints on dark matter annihilation into gamma rays

Gregory D. Mack,[1,2] Thomas D. Jacques,[3] John F. Beacom,[1,2,4] Nicole F. Bell,[3] and Hasan Yüksel[1,2]

[1]*Department of Physics, Ohio State University, Columbus, Ohio 43210*

[2]*Center for Cosmology and Astro-Particle Physics, Ohio State University, Columbus, Ohio 43210*

[3]*School of Physics, The University of Melbourne, Victoria 3010, Australia*

[4]*Department of Astronomy, Ohio State University, Columbus, Ohio 43210*

(Received 5 May 2008; published 26 September 2008)

Using gamma-ray data from observations of the Milky Way, Andromeda (M31), and the cosmic background, we calculate conservative upper limits on the dark matter self-annihilation cross section to monoenergetic gamma rays, $\langle \sigma_A v \rangle_{\gamma\gamma}$, over a wide range of dark matter masses. (In fact, over most of this range, our results are unchanged if one considers just the branching ratio to gamma rays with energies within a factor of a few of the endpoint at the dark matter mass.) If the final-state branching ratio to gamma rays, $\mathrm{Br}(\gamma\gamma)$, were known, then $\langle \sigma_A v \rangle_{\gamma\gamma}/\mathrm{Br}(\gamma\gamma)$ would define an upper limit on the *total* cross section; we conservatively assume $\mathrm{Br}(\gamma\gamma) \gtrsim 10^{-4}$. An upper limit on the total cross section can also be derived by considering the appearance rates of *any* standard model particles; in practice, this limit is defined by neutrinos, which are the least detectable. For intermediate dark matter masses, gamma-ray-based and neutrino-based upper limits on the total cross section are comparable, while the gamma-ray limit is stronger for small masses and the neutrino limit is stronger for large masses. We comment on how these results depend on the assumptions about astrophysical inputs and annihilation final states, and how GLAST and other gamma-ray experiments can improve upon them.

DOI: 10.1103/PhysRevD.78.063542 PACS numbers: 95.35.+d, 95.85.Pw, 98.62.Gq, 98.70.Vc

I. INTRODUCTION

While there is ample gravitational evidence for dark matter, the nature of these particles remains mysterious and is defined principally by the weakness of their interactions; for reviews, see e.g., Refs. [1–3]. The dark matter self-annihilation cross section is of particular importance, since dark matter concentrations will produce gamma rays and other detectable standard model (SM) particles. If the dark matter (DM) is a thermal relic of the early universe, the annihilation cross section must be $\langle \sigma_A v \rangle \sim 3 \times 10^{-26}\ \mathrm{cm^3\ s^{-1}}$ in order to obtain the observed relic abundance, $\Omega_{\mathrm{DM}} \simeq 0.3$. (Throughout, we consider this cross section averaged with velocity over the dark matter velocity distribution; in the Milky Way, $v_{\mathrm{rms}} \sim 10^{-3} c$.) It is possible that dark matter is not a thermal relic, e.g., Refs. [4,5], which makes it even more interesting to consider direct late-universe constraints on the annihilation cross section, e.g., Refs. [1–3,6–12].

Even if the *total* annihilation cross section is set by the relic abundance, the branching ratios to specific final states are model dependent. The dark matter disappearance rate due to annihilation can be constrained by the appearance rates of various SM particles. If the dark matter is the lightest stable particle in some new physics sector, then it can be natural to have the final-state branching ratio to SM particles, Br(SM), be 100%, as we assume. If the final states include new and purely sterile particles, then all appearance-based results are weakened proportionally to Br(SM).

We assume that annihilation is not prevented in principle by dark matter not being its own antiparticle, or in practice by a large particle-antiparticle asymmetry. We also assume that a single type of new particle comprises the dark matter that is required to exist in the present-day universe, and that, consistent with observations, the density distributions of dark matter halos are not appreciably affected by possible dark matter interactions. These assumptions are made implicitly in nearly all papers about dark matter annihilation.

Here we calculate the constraints that can be placed on the annihilation cross section using gamma rays, the most detectable final states, over a wide range of dark matter masses. We first focus on the $\gamma\gamma$ final state, as it would be a very clean signature of dark matter annihilation, with $E_\gamma = m_\chi$, e.g., Refs. [13–19]. Unfortunately, in typical models, this is small, $\mathrm{Br}(\gamma\gamma) \sim 10^{-4}$–$10^{-3}$; in some models, it can be larger [20–22], but one cannot be certain that these predictions match with nature. Since gamma rays will be ubiquitously produced, directly in SM final states, or through radiative corrections and energy-loss processes, we also consider more general outcomes, in which the gamma-ray energies are in a broader range below m_χ.

We consider constraints on the dark matter annihilation cross section over a large mass range of 10^{-5}–10^{5} GeV. At all but the highest energies, gamma-ray data is available to test the annihilation cross section, provided that we combine constraints defined using the Milky Way halo, the Andromeda halo, and all the halos in the universe. (Modern data, especially those from observations of the Milky Way and Andromeda, are significantly more constraining than those that were available earlier, e.g., at the time of Ref. [23], which considered limits on the decay of

an unstable massive neutrino.) We hope that our results will be useful in challenging experiments to report stronger limits using new data and focused analyses. With the launch of GLAST this year, and with new studies by TeV-range experiments, these prospects are good. Using our upper limits on the dark matter annihilation cross section to gamma rays, and a conservative assumption about the branching ratio to monoenergetic gamma rays, we define upper limits on the total cross section and compare to other constraints.

Since the dark matter annihilation rate scales with density squared and the density profiles are uncertain, we are mindful of how our constraints on the cross section are affected by astrophysical uncertainties. We are conservative in our input choices and analysis methods, and we show how our results depend on these. In light of these considerations, we do not consider corrections that would affect the results by less than a factor of ~ 2, which also allows some simplifications. Our upper bounds on the annihilation cross section to gamma rays would only be improved by more optimistic assumptions.

In Sec. II, we discuss important general bounds on the total annihilation cross section. In Sec. III, we review the analysis methods used for the case of gamma-ray lines from various dark matter concentrations. The experiments and observations we use are discussed in Sec. IV. In Sec. V, we summarize and interpret our results.

II. CROSS SECTION CONSTRAINTS

The annihilation cross section sets the dark matter *disappearance* rate, for which there are two important constraints. The first is unitarity [24,25], which sets a general upper bound that can only be evaded in unusual cases [26]. In the low-velocity limit, where s-wave annihilation dominates, the unitarity bound is $\langle \sigma_A v \rangle < 4\pi/m_\chi^2 v$, or

$$\langle \sigma_A v \rangle \leq (1.5 \times 10^{-13}\ \mathrm{cm^3\,s^{-1}}) \left[\frac{300\ \mathrm{km/s}}{v_{\mathrm{rms}}}\right] \left[\frac{\mathrm{GeV}}{m_\chi}\right]^2. \quad (1)$$

For $m_\chi \gtrsim 10^6$ GeV, this would require that $\langle \sigma_A v \rangle$ be smaller than that for a thermal relic, and which would thus give too large of a relic abundance [24]. However, for smaller m_χ the unitarity limit is much less constraining. The second general constraint comes from the requirement that annihilation does not drastically alter the density profiles of dark matter halos in the Universe today. In the model of Kaplinghat, Knox, and Turner (KKT) [4], a large self-annihilation cross section was invoked in order to reconcile predicted cuspy density profiles with the flatter ones inferred from observation, requiring

$$\langle \sigma_A v \rangle_{\mathrm{KKT}} \simeq (3 \times 10^{-19}\ \mathrm{cm^3\,s^{-1}}) \left[\frac{m_\chi}{\mathrm{GeV}}\right]. \quad (2)$$

We reinterpret this result as an approximate upper bound, beyond which halo density profiles would be significantly distorted by dark matter annihilation. Note that this limit is very weak for all but the lightest masses.

We now discuss limits which arise from the *appearance* rate of dark matter annihilation products, assuming Br(SM) = 100%. All final states except neutrinos obviously produce gamma rays, either directly or as secondary particles (we return to neutrinos next). Quarks and gluons hadronize, producing pions and thus photons via $\pi^0 \rightarrow \gamma\gamma$, while $\tau^\pm$, $W^\pm$, and Z^0 also produce π^0 via their decays. Charged particles produce photons via electromagnetic radiative corrections [27], and electrons and positrons also produce photons via energy-loss processes [28]. Therefore, we expect a broad spectrum of final-state photons, even though the branching ratio to the monoenergetic $\gamma\gamma$ final state may be small. We use the gamma-ray data to place upper limits on $\langle \sigma_A v \rangle_{\gamma\gamma}$, and these are of general interest for their own sake. With an assumption about Br($\gamma\gamma$), these results also define an upper limit on the total cross section of $\langle \sigma_A v \rangle_{\gamma\gamma}/\mathrm{Br}(\gamma\gamma)$. Unless one is confident that Br($\gamma\gamma$) cannot be too small, then this constraint on the total cross section can be arbitrarily weakened.

An important general limit on the *total* annihilation cross section can be obtained by considering annihilation into the *least* detectable final state, namely, neutrinos [7,8]. Given that stronger constraints will exist on all final states other than neutrinos, we can set a conservative upper bound on the total dark matter annihilation rate by assuming the branching ratio to neutrinos is 100%. (Unlike all other constraints, the neutrino constraint, being the weakest, is not to be divided by a realistic branching ratio; this follows from the fact that the sum of all branching ratios must be 100%.) The resulting limits are surprisingly strong. Dark matter annihilation into neutrinos was explored by Beacom, Bell, and Mack (BBM) [7], and Yüksel *et al.* (YHBA) [8], for cosmic and Galactic dark matter sources, respectively. By requiring that the neutrino flux produced by annihilation be smaller than the measured atmospheric neutrino background, robust bounds on the total annihilation cross section were obtained over a wide mass range. (Reference [29] extended the dark matter annihilation limits to lower masses and Ref. [30] developed analogous dark matter decay limits over a wide range of masses.) For all masses considered, these limits are much stronger than the KKT limit; they are also stronger than the unitarity limit except at high masses. While neutrinos are the least detectable annihilation products, even they are accompanied by gamma rays via electroweak radiative corrections; these results lead to constraints on $\langle \sigma_A v \rangle$ that are comparable to or better than those obtained directly with neutrinos [9–11].

III. CALCULATION OF DARK MATTER SIGNALS

The dark matter annihilation rate depends on the square of the dark matter number density ρ/m_χ, which is written

in terms of the unknown mass m_χ and the uncertain dark matter mass density ρ. Not coincidentally, where the density is largest, at the centers of halos, the uncertainties are the largest; these regions contribute relatively little to the gravitationally measured mass of a halo. To cover as large of an energy range as possible, we have to consider gamma-ray data for the Milky Way, Andromeda, and all of the dark matter halos in the Universe. In all cases, though the astrophysical and analysis uncertainties vary in their severity, we make conservative choices for the dark matter density and hence the cross section limits (smaller choices for the density mean larger upper limits on the cross section).

A. Dark matter halos

A standard parameterization of the dark matter density profile in a halo is

$$\rho(r) = \frac{\rho_0}{(r/r_s)^\gamma[1 + (r/r_s)^\alpha]^{(\beta-\gamma)/\alpha}}. \quad (3)$$

The Navarro-Frenk-White (NFW) [31] and Kravtsov profiles [32] are defined by $(\alpha, \beta, \gamma) = (1, 3, 1)$ and $(\alpha, \beta, \gamma) = (2, 3, 0.4)$, respectively. Near the center of the halo, the density of an NFW profile scales with radius as $1/r$, while the Kravtsov profile scales less steeply, as $1/r^{0.4}$. For large radii, $r \gtrsim r_s$, these two profiles coincide more closely. For the Milky Way, r_s is 20 kpc for the NFW profile and 10 kpc for the Kravtsov profile, while the normalization, ρ_0, is fixed such that the density at the solar circle distance, $R_{\rm sc} = 8.5$ kpc, is $\rho(R_{\rm sc}) = 0.3$ GeV cm^{-3} (0.37 GeV cm^{-3}) for the NFW (Kravtsov) profile.

There does not appear to be a consensus on the values of the halo parameters for Andromeda; for example, compare the NFW profiles in Ref. [33] with Ref. [34], where both ρ_0 and r_s are quite different. Thus we have chosen to model Andromeda using the Milky Way parameters, as an appropriate compromise between competing extremes.

In the innermost regions of halos, the uncertainties in the dark matter density and thus the annihilation rate are at their largest. For larger central regions, or whole halos, these uncertainties are much less. For the Milky Way, these effects can easily be seen in Fig. 2 of YHBA; for larger angular regions centered on the Galactic Center, the dark matter annihilation signals for different profiles become much more similar to each other. While the uncertainties at small angular scales can be orders of magnitude, those at large angular scales are not more than a factor of about 2.

In YHBA, we explored in detail how various annihilation signals depend on the choice of dark matter density profile. Our overall approach is to be conservative by adopting smaller choices of the astrophysical inputs; this means that larger values of the cross section would be required to get the same gamma ray or neutrino fluxes. Here we use the Kravtsov profile for our main results; for the commonly-adopted NFW profile, we find smaller (more restrictive) upper bounds on the cross sections, as shown below. Also to be conservative, we neglect the possibility of halo substructure, e.g., Refs. [35,36], or mini-spikes around intermediate-mass black holes [37,38], which would lead to enhanced annihilation signals.

B. Milky way and Andromeda signals

We first consider annihilations in our Galaxy, following the conventions of YHBA, and generalize this to the nearby galaxy Andromeda (M31). The intensity (flux per solid angle) of the annihilation signal at an angle ψ with respect to the Galactic Center (GC) is proportional to the square of the dark matter density integrated over the line of sight,

$$\mathcal{J}(\psi) = \mathrm{J}_0 \int_0^{\ell_{\rm max}} \rho^2\left(\sqrt{R_{\rm sc}^2 - 2\ell R_{\rm sc}\cos\psi + \ell^2}\right) d\ell, \quad (4)$$

where $\mathrm{J}_0 = 1/[8.5\ \mathrm{kpc} \times (0.3\ \mathrm{GeV\,cm^{-3}})^2]$ is an arbitrary normalization we use to make $\mathcal{J}$ a dimensionless quantity, and which cancels in the final results. The upper limit of the integration is given by $\ell_{\rm max} = (R_{\rm MW}^2 - \sin^2\psi R_{\rm sc}^2)^{1/2} + R_{\rm sc}\cos\psi$. We define $\mathcal{J}_{\Delta\Omega}$ as the average of $\mathcal{J}$ over a cone of half-angle ψ centered on the GC,

$$\mathcal{J}_{\Delta\Omega} = \frac{2\pi}{\Delta\Omega}\int_0^\psi \mathcal{J}(\psi)\sin\psi d\psi, \quad (5)$$

where $\Delta\Omega = 2\pi(1 - \cos\psi)$ is the angular size of the cone in steradians. The values of $\mathcal{J}(\psi)$ and $\mathcal{J}_{\Delta\Omega}$ can be read directly from Fig. 2 of YHBA [below, we do not explicitly show the sr^{-1} units of $\mathcal{J}(\psi)$ and $\mathcal{J}_{\Delta\Omega}$].

Equation (4) can easily be generalized to external halos [39,40] (such as the Andromeda galaxy at a distance of $D_{\rm M31} \simeq 700$ Mpc) using

$$\mathcal{J}(\psi) = \mathrm{J}_0 \int_{\ell_{\rm min}}^{\ell_{\rm max}} \rho^2\left(\sqrt{D_{\rm M31}^2 - 2\ell D_{\rm M31}\cos\psi + \ell^2}\right) d\ell, \quad (6)$$

where the result is independent of the upper and lower limits of integration $(\ell_{\rm min}, \ell_{\rm max})$ as long as they cover most of the halo under consideration.

For extragalactic dark matter sources, the annihilation signals will include a contribution from the dark matter in our own galaxy along the line of sight. However, in the case of an external galaxy like Andromeda, this contribution will be eliminated if there is a subtraction of the background intensity from a region close to the source, as is often done in observational analyses.

With these definitions, the intensity of the dark matter annihilation gamma-ray signal is

$$\frac{d\Phi_\gamma}{dE} = \frac{\langle\sigma_A v\rangle}{2}\frac{\mathcal{J}_{\Delta\Omega}}{\mathrm{J}_0}\frac{1}{4\pi m_\chi^2}\frac{dN_\gamma}{dE}, \quad (7)$$

where dN_γ/dE is the gamma-ray spectrum per annihilation. In the case of annihilation into two monoenergetic

gamma rays, we simply have $dN_\gamma/dE = 2\delta(m_\chi - E)$; we generalize this below. Similarly, the total flux (per unit energy) from a region of solid angle $\Delta\Omega$ is

$$\frac{d\phi_\gamma}{dE} = \frac{d\Phi_\gamma}{dE}\Delta\Omega = \frac{\langle\sigma_A v\rangle}{2}\frac{\mathcal{J}_{\Delta\Omega}\Delta\Omega}{\mathrm{J}_0}\frac{1}{4\pi m_\chi^2}\frac{dN_\gamma}{dE}. \quad (8)$$

C. Cosmic diffuse signal

The calculation of the cosmic diffuse annihilation signal is detailed, for example, in Refs. [6,41], where the cosmological flux of annihilation products from external galaxies was calculated taking the clustering of dark matter into account. Recently, BBM and YHBA applied this technique to the scenario where dark matter annihilates into neutrinos.

The cosmic diffuse flux, arising from dark matter annihilation in halos throughout the Universe, is

$$\frac{d\Phi_\gamma}{dE} = \frac{\langle\sigma_A v\rangle}{2}\frac{c}{4\pi H_0}\frac{\Omega_{\mathrm{DM}}^2\rho_{\mathrm{crit}}^2}{m_\chi^2} \times \int_0^{z_{\mathrm{up}}}\frac{f(z)(1+z)^3}{h(z)}\frac{dN_\gamma(E')}{dE'}e^{-z/z_{\mathrm{max}}}dz, \quad (9)$$

where $H_0 = 70\ \mathrm{km\,s^{-1}\,Mpc^{-1}}$ is the Hubble parameter and Ω_{DM} is the dark matter density in units of the critical density. We assume a flat universe, with $\Omega_{\mathrm{DM}} = 0.3$, $\Omega_\Lambda = 0.7$, $h(z) = [(1+z)^3\Omega_{\mathrm{DM}} + \Omega_\Lambda]^{1/2}$. The factor $e^{-z/z_{\mathrm{max}}}$, taken from Ref. [6], accounts for the attenuation of gamma rays, a modest effect for the energies considered here. The factor $f(z)$ in Eq. (9) accounts for the average increase in density squared due to the fact that dark matter is clustered into halos, rather than uniformly distributed, and the evolution with redshift of the halo number density. [The Δ^2 factor in BBM is equal to $f(z)(1+z)^3$.] Following YHBA, we use the parameterization $\log_{10}(f(z)/f_0) = 0.9[\exp(-0.9z) - 1] - 0.16z$, where f_0 depends on the halo profile. Choosing the Kravtsov (NFW) profile, $f_0 \simeq 2(5) \times 10^4$.

Gamma rays that are produced with energy E' are observed with redshifted energy $E = E'/(1+z)$. For annihilation into monoenergetic gamma rays, the delta function source spectrum is modified by redshift as

$$\frac{dN}{dE'} = 2\delta(m_\chi - E') = \frac{2}{E}\delta\left(z - \left(\frac{m_\chi}{E} - 1\right)\right), \quad (10)$$

which shows that the observed flux at an energy E is contributed by sources at redshift $\frac{m_\chi}{E} - 1$.

IV. SPECIFIC OBSERVATIONS AND DERIVED ANNIHILATION CONSTRAINTS

We have collected gamma-ray flux measurements and limits from a wide variety of experiments, spanning an extensive energy range from 20 keV to 10 TeV. In most of the observations, the energy spectra are given in log-spaced energy intervals. We calculate annihilation gamma-ray fluxes for the Galactic, Andromeda, and cosmic dark matter sources, using the methods outlined in Sec. III above. These are compared with observational data over an energy range, conveniently chosen as $10^{-0.4}m_\chi$–m_χ, that is comparable to or larger than the energy resolution and bin size of the experiments. If only upper limits on the flux are given, we instead compare our predictions directly with these upper limits.

Our constraints on the dark matter annihilation rate are conservatively determined by demanding that the annihilation flux be smaller than 100% of the observed (presumably not produced by dark matter) gamma-ray background flux at the corresponding energy range. In Fig. 1, we show the GC and cosmic diffuse signals from dark matter annihilations which fulfill this criterion, superimposed upon the Galactic and extragalactic spectra, respectively, as measured by COMPTEL and EGRET.

The experiments report their results as either intensity [as in Eq. (7)], which requires that we calculate $\mathcal{J}_{\Delta\Omega}$, or flux from a given angular region [as in Eq. (8)], for which we need $\mathcal{J}_{\Delta\Omega}\Delta\Omega$. We present the values of these parame-

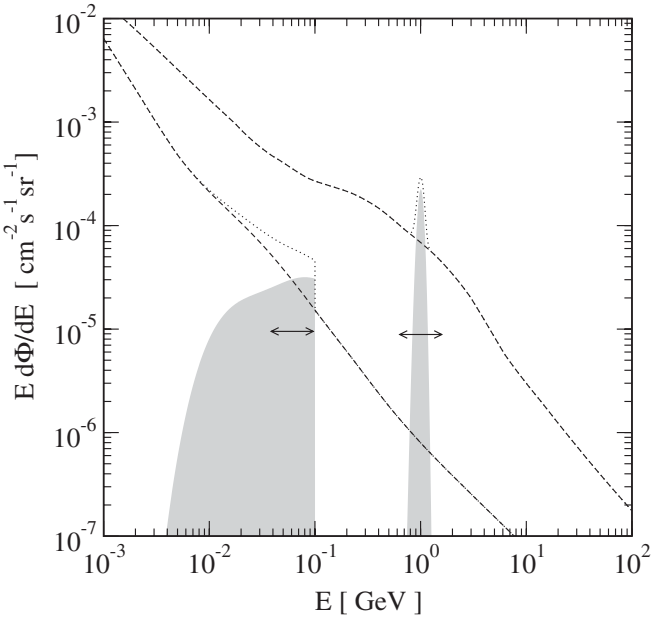

FIG. 1. Example dark matter annihilation signals, shown superimposed on the Galactic and extragalactic gamma-ray spectra measured by COMPTEL and EGRET. In each case, the cross section is chosen so that the signals are normalized according to our conservative detection criteria, namely, that the signal be 100% of the size of the background when integrated in the energy range chosen (0.4 in $\log_{10}E$, shown by horizontal arrows). The narrow signal on the right is the Galactic Center flux due to annihilation into monoenergetic gamma rays, for $m_\chi = 1$ GeV; the signal is smeared as appropriate for a detection with finite energy resolution. The broad feature on the left is the cosmic diffuse signal for annihilation into monoenergetic gamma rays at $m_\chi = 0.1$ GeV, smeared by redshift.

ters which correspond to the Kravtsov profile, as this results in the most conservative upper limits on the annihilation cross section. Our limits on the dark matter annihilation cross section are reported in Fig. 2, where we also show how our results would change if the NFW profile were adopted instead. The details of the experiments and our analyses are summarized below for each observation.

A. COMPTEL and EGRET

COMPTEL [42], the imaging COMPton TELescope aboard the Compton Gamma Ray Observatory (CGRO) satellite, measured gamma rays in the energy range 1–30 MeV. EGRET [43], the Energetic Gamma Ray Experiment Telescope, also aboard the CGRO, measured gamma rays in the energy range 30 MeV to nearly 100 GeV. For both COMPTEL and EGRET, the full sky was studied with an angular resolution of at worst a few degrees (for the large regions we consider, this makes no difference). The energy resolution was modest, and the data were given in a few logarithmically spaced bins per decade in energy.

Both COMPTEL and EGRET observed the Galactic Center region, and the measured gamma-ray intensity energy spectra are reported in Ref. [44,45] for the region $-30^\circ < l < 30^\circ$ and $-5^\circ < b < 5^\circ$ (Galactic longitude and latitude, respectively). The disklike morphology of the emission region makes it clear that nearly all of this emission is due to ordinary astrophysical sources; to be conservative, we do not attempt to define a limit on the small component of this that could be due to centrally concentrated dark matter, and simply use the total observed intensity to bound any dark matter contribution. Also, we evaluate the dark matter signal as if from a circular region of $\psi = 30^\circ$; accounting for the rectangular shape of the region would lead to a higher value than the $\mathcal{J}_{\Delta\Omega} \simeq 13$ that we adopt. Using a less conservative set of assumptions than we employ, stronger limits on $\langle\sigma v\rangle_{\gamma\gamma}$ were derived from the EGRET data in Ref. [15].

B. H.E.S.S.

H.E.S.S. (High Energy Stereoscopic System), a system of multiple atmospheric Čerenkov telescopes, is presently in operation in Namibia [46]. H.E.S.S. observed the Galactic Center region in the energy range 0.3–15 TeV. An apparent point source at the Galactic Center was observed, as was an extended source ($\sim 1^\circ$) known as the Galactic Center Ridge [47]. While the origin of the point source is unknown, the Ridge emission is almost certainly astrophysical, and is consistent with being caused by cosmic rays colliding with a gas cloud (again, we do not attempt to account for this, and will simply bound any dark matter contribution by the total observed intensity).

Since the uncertainties in the dark matter profile increase for smaller angular regions around the Galactic Center, it is more robust to define our results using the extended region instead of the point source. The Ridge emission was observed in an angular region $-0.8^\circ < l < 0.8^\circ$ and $-0.3^\circ < b < 0.3^\circ$ in Galactic coordinates, and the resulting flux reported by H.E.S.S. reflected a background subtraction from a nearby region ($-0.8^\circ < l < 0.8^\circ$ and $0.8^\circ < b < 1.5^\circ$) to help account for cosmic rays. Thus, we have to consider not the whole dark matter signal, but just its contrast between the central and adjacent regions by accounting for this subtraction in our analysis.

We approximate the intensity from the rectangular region of the Galactic Center Ridge with a circle of radius 0.8°. We also estimate the adverse effect of the background subtraction on our limits by choosing $\mathcal{J}$ to be subtracted at its maximum, i.e., $\psi = 0.8^\circ$. This means

$$\mathcal{J}_{\Delta\Omega} = \frac{2\pi}{\Delta\Omega}\int_0^{0.8^\circ} (\mathcal{J}(\psi) - \mathcal{J}(0.8^\circ))\sin\psi d\psi \simeq 3. \quad (11)$$

Had we not made this subtraction correction, our limits on the cross section would be stronger by about an order of magnitude.

C. INTEGRAL

The space-borne INTEGRAL (INTErnational Gamma-Ray Astrophysics Laboratory) observatory [48] has searched for gamma-ray emission in the Milky Way over the energy range 20–8000 keV, using the SPectrometer on INTEGRAL (SPI). Teegarden and Watanabe [49] presented results of an INTEGRAL search for gamma-ray line emission from the Galactic Center region (we use their zero-intrinsic-width results, as appropriate for the low dark matter velocities of the halo). Other than the expected positron annihilation [50] and ^{26}Al decay [51] signatures, no evidence of other line emission was found.

To reduce backgrounds and improve the sensitivity of the line search, the measured intensity from large angular radii ($> 30^\circ$) was subtracted from that in the Galactic Center region ($< 13^\circ$), resulting in a 3.5–σ constraint on the flux of very roughly $\lesssim 10^{-4}$ photons cm^{-2} s^{-1} in the energy range 20–8000 keV. Our calculations must reflect this subtraction, which will somewhat weaken the sensitivity to the dark matter signal. A similar correction was used in Ref. [52]. We implement this as

$$\mathcal{J}_{\Delta\Omega}\Delta\Omega = 2\pi\int_0^{13^\circ} (\mathcal{J}(\psi) - \mathcal{J}(>30^\circ))\sin\psi d\psi \simeq 2. \quad (12)$$

Because of the decreasing trend of the dark matter profile, the intensity outside the Galactic Center region will be largest at 30°, and accordingly we choose this value to be as conservative as possible (a larger subtraction leads to a weaker upper limit on $\langle\sigma_A v\rangle$). Had we not made this correction, our limits on the cross section would be stronger by about a factor of 2.

D. Andromeda halo results

The Andromeda galaxy (M31) has been observed by several gamma-ray experiments, all of which placed upper limits on the flux. EGRET, CELESTE, and HEGRA all observed Andromeda, each encompassing a, respectively, smaller angular region of that extended object. As the results were reported as flux limits from specified angular regions, we compare to these using $\mathcal{J}_{\Delta\Omega}\Delta\Omega$, which is an input to Eq. (8).

EGRET viewed Andromeda with an angular radius of 0.5° and set a 2–σ upper limit on the gamma-ray flux of 1.6×10^{-8} photons cm^{-2} s^{-1} from 0.1 GeV to 2 GeV, since no signal was seen [53]. For the angular region of this observation, the flux will be proportional to

$$\mathcal{J}_{\Delta\Omega}\Delta\Omega = 2\pi \int_0^{0.5^\circ} \mathcal{J}'(\psi) \sin\psi d\psi \simeq 2 \times 10^{-3}. \quad (13)$$

CELESTE (ČErenkov Low Energy Sampling and Timing Experiment) is an atmospheric Čerenkov telescope in the French Pyrenees, which studies gamma rays with energies greater than 50 GeV [54]. It viewed Andromeda in the energy range of 50–700 GeV, and again no signal was seen [55]. A 2–σ upper limit on the energy-integrated flux from Andromeda was reported as $\lesssim 10^{-10}$ photons cm^{-2} s^{-1}; employing an angular radius of $\theta_{\rm obs} = 0.29^\circ$ yields $\mathcal{J}_{\Delta\Omega}\Delta\Omega \simeq 1 \times 10^{-3}$.

HEGRA (High Energy Gamma Ray Astronomy experiment) was an atmospheric Čerenkov telescope, located in La Palma in the Canary Islands [56]. It took data in the range 0.5–10 TeV, with better energy resolution than that of CELESTE [57]. It used an even smaller angular radius of $\theta_{\rm obs} = 0.105^\circ$, which yields $\mathcal{J}_{\Delta\Omega}\Delta\Omega \simeq 2 \times 10^{-4}$. HEGRA reported 99% C.L. upper limits for the gamma-ray line flux, and these can be used directly.

E. Cosmic diffuse results

INTEGRAL [58], COMPTEL [59], and EGRET [60] have all made measurements of the gamma-ray flux at high latitudes, and these can be used to set a limit on the cosmic dark matter annihilation signal. The INTEGRAL data used here were those collected in broad energy bins, much like those of COMPTEL and EGRET. The cosmic gamma-ray background was also measured by the Gamma-Ray Spectrometer aboard the Solar Maximum Mission (SMM) [61] over the energy range 0.3–8 MeV, for a field of view of 135° in the direction of the Sun [62], and we include this data.

For the cosmic diffuse analysis, the framework detailed in Sec. III C can be applied. Note that for simplicity we calculate only the true cosmic diffuse dark matter signal, neglecting any Galactic contribution along the lines of sight. This contribution from the Galactic halo (which would add to the signal and thus make our limits stronger) is significant for NFW or steeper profiles and can even dominate over the true cosmic dark matter signal; see YHBA and Ref. [63].

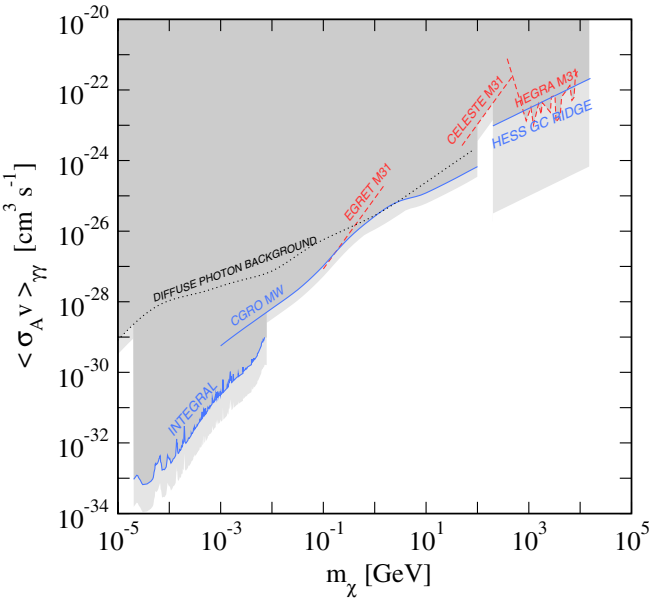

FIG. 2 (color online). The limits on the partial cross section, $\langle\sigma_A v\rangle_{\gamma\gamma}$, derived from the various gamma-ray data. Our overall limit is shown as the dark shaded exclusion region. For comparison, the light-shaded region shows the corresponding limits for the NFW (rather than the Kravtsov) profile.

V. DISCUSSION AND CONCLUSIONS

A. Limits on the cross section to gamma rays

In Fig. 2, we combine all of the upper limits on the partial cross section to monoenergetic gamma rays, choosing the strongest limit for each value of the dark matter mass. The shaded exclusion region shows our combined bound. These searches for dark matter signals are limited by astrophysical backgrounds, and the general trend of how the limits vary with mass follows from how these backgrounds vary with energy. We can estimate how the cross section limit should scale with mass, and how it should depend on the assumed spectrum of final-state gamma rays and the choice of density profile.

Recall that we conservatively require the signal to be as large as the full measured background in an energy bin. The gamma-ray number flux of the signal integrated in a logarithmic energy bin $\Delta(\ln E)$ scales as $E d\Phi/dE\,\Delta(\ln E) \sim \langle\sigma_A v\rangle/m_\chi^2$, provided that the bin is wide enough to contain the full signal. The gamma-ray number flux of the background integrated in the same logarithmic energy bin scales as $E d\Phi/dE\,\Delta(\ln E) \sim E/E^\alpha\,\Delta(\ln E)$, for a background spectrum $d\Phi/dE \sim 1/E^\alpha$. For a narrow bin, the evaluation point is $E \sim m_\chi$. We then expect the upper limit on the cross section to scale as $\langle\sigma_A v\rangle_{\rm limit} \sim m_\chi^{3-\alpha}\,\Delta(\ln E)$. For example, for the EGRET diffuse data, α is slightly greater than 2, and so the cross

section limits in this energy range scale slightly less rapidly than as $\langle\sigma_A v\rangle_{\rm limit} \sim m_\chi$.

Most of these experiments had modest energy resolution. To be conservative, we assume an analysis bin with a logarithmic energy width of 0.4 in $\log_{10}E$ [i.e., $\Delta(\ln E) \sim 1$] for the Galactic and cosmic diffuse analyses; this is at least as wide as the energy bins reported by the experiments. That is, even though we nominally assume two monoenergetic gamma rays at $E_\gamma = m_\chi$, our results have not taken advantage of this fact. In effect, our results are what one would obtain for an annihilation gamma-ray spectrum as wide as 0.4 in $\log_{10}E$. The exception is the INTEGRAL line search, where the excellent energy resolution is what leads to this limit being stronger than expected from the general trend in Fig. 2.

Because of radiative corrections [27] or energy-loss processes [28], there should be some gamma rays near the endpoint, and our results can be scaled if the assumed branching ratio is less than the 100% used in Fig. 2. For example, for charged-particle final states, the branching ratio to internal bremsstrahlung gamma rays near the endpoint is $\mathrm{Br}(\gamma) \sim \alpha \sim 10^{-2}$. For neutral final states, there will typically be gamma rays (or neutrinos) near the endpoint. To be conservative about these details, we chose a nominal minimum branching ratio to gamma rays near the endpoint of 10^{-4}.

How would our results change if we considered an even broader annihilation gamma-ray spectrum? We emphasize that the results shown in Fig. 2, which are based on direct numerical integration, are already valid for spectra as wide as our analysis bins. First, we should take into account the increase in the logarithmic bin width. Second, to be more precise, the evaluation point for the background spectrum should not be $E = m_\chi$, but rather $E = m_\chi/a$, with $a > 1$. This increases the estimate of the integrated background, and hence the cross section limit, by a factor $\sim a^{\alpha-1}$. Thus, if we took the annihilation gamma-ray spectrum to be as much as 1 order of magnitude wide, then our limits in Fig. 2 would be weakened by at most a factor of several, depending on the background spectrum. (For the INTEGRAL line search, the correction would be much larger.)

Given the large range on the axes in Fig. 2, and our intention to define approximate and conservative limits, this shows that our results are much more general than they first appear. Similarly, the results in BBM [7] and YHBA [8] do not have a strong dependence on the assumed annihilation neutrino spectrum.

How sensitive are our limits to the choice of density profile? As noted, we chose the rather shallow Kravtsov profile to be conservative. If we were to adopt an NFW profile, which increases much more rapidly toward the Galactic Center (scaling with radius as r^{-1} rather than $r^{-0.4}$) the annihilation rates would be larger and the cross section limits correspondingly stronger. In Fig. 2, we show how our results would change if we had used an NFW profile instead of the Kravtsov profile. At most energies, the changes are modest, and illustrative of the potential uncertainties. The only significant change to the combined gamma-ray limit is for the H.E.S.S. Galactic Center Ridge case, which is based on small angular radii. In the NFW case, the steeper profile gives an overall larger intensity and a smaller signal cancellation when the background is subtracted. A fuller discussion of how the annihilation signals depend on the choice of dark matter density profile is given in YHBA.

B. Limits on the total cross section

Unsurprisingly, the cross section bounds derived under the assumption of monoenergetic gamma rays are substantially stronger than those defined similarly for final-state neutrinos in BBM [7] and YHBA [8]. (At the highest masses, near 10^4 GeV, this is no longer true, first because of how the numerical limits work out, and then because we do not presently have good gamma-ray data or limits at higher energies; we expect that dedicated analyses by H.E.S.S. and other experiments will soon improve this.) Indeed, this was an assertion in those two works that we have now justified in more detail than before.

It is unrealistic to have $\mathrm{Br}(\gamma\gamma) = 100\%$, of course, if one is trying to set a limit on the *total* cross section. If $\mathrm{Br}(\gamma\gamma)$ is known, then a limit on the total cross section can be determined by dividing the limit on the partial cross section to that final state by the branching ratio:

$$\langle\sigma_A v\rangle_{\rm total} = \frac{\langle\sigma_A v\rangle_{\gamma\gamma}}{\mathrm{Br}(\gamma\gamma)}. \tag{14}$$

In typical models, this branching ratio is typically 10^{-3} or smaller [1–3]. To be conservative, we must just choose a value such that it is implausible that the true branching ratio could be smaller. We therefore assume $\mathrm{Br}(\gamma\gamma) = 10^{-4}$, but this choice could be debated. As noted, our analysis uses wide logarithmic energy bins, and so, at the very least, would capture the gamma rays near the endpoint due to internal bremsstrahlung from charged particles [27]. [Similarly, as a general point, limits on the total cross section defined by assuming only W^+W^- final states [12] would have to be corrected by dividing by $\mathrm{Br}(W^+W^-)$.]

Figure 3 summarizes various limits on the total cross section, including the one just described, the unitarity bound mentioned earlier, and the neutrino bound from YHBA (based on the Milky Way signal and the Kravtsov profile). The standard cross section for a thermal relic is also shown. Note that our limits bound $\langle\sigma_A v\rangle$ directly, independent of whether σ_A is s-wave or p-wave dominated. These results, combined with those in Fig. 2, strongly constrain the possibilities for large dark matter annihilation signals, e.g., as assumed in Ref. [64].

When shown in this way, it becomes clear how surprisingly strong the neutrino bound on the *total* cross section

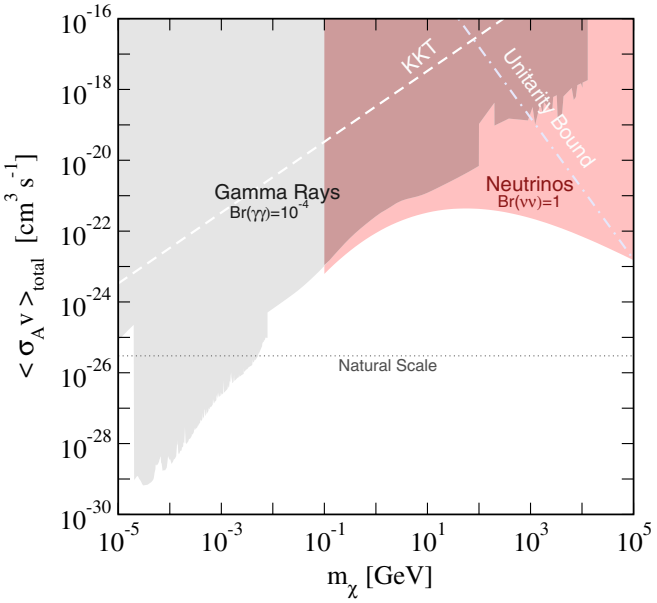

FIG. 3 (color online). The gamma-ray and neutrino limits on the total annihilation cross section, selecting $\mathrm{Br}(\gamma\gamma) = 10^{-4}$ as a conservative value. The unitarity [24,25] and KKT [4] bounds are also shown. The overall bound on the total cross section at a given mass is determined by the strongest of the various upper limits.

is, as it is comparable to the bound obtained using the gamma-ray flux limits and a reasonable assumption about the minimum branching ratio to gamma rays. It is very important to emphasize that while the gamma-ray bound on the partial cross section had to be divided by a realistic $\mathrm{Br}(\gamma\gamma)$, this is *not* the case for the neutrino bound, as explained above. If we assume only SM final states, then all final states besides neutrinos lead to appreciable fluxes of gamma rays, and hence are more strongly excluded. Of course, the gamma-ray and neutrino cross section limits can both be weakened by assuming an appreciable branching ratio to new and truly sterile particles.

C. Conclusions and prospects

Using gamma-ray data from a variety of experiments, we have calculated upper limits on the dark matter annihilation cross section to gamma rays over a wide range of masses. These limits are conservatively defined, in terms of our analysis criteria, our assumptions about the uncertain dark matter density profiles, and the gamma-ray spectrum. While our results were nominally defined for monoenergetic gamma rays with $E_\gamma = m_\chi$, we have shown that all of our results except the INTEGRAL line flux limit are only weakly dependent on this assumption. The limits obtained for more general gamma-ray spectra would only be somewhat less stringent.

There are good prospects for improved sensitivity with present and upcoming gamma-ray experiments, particularly GLAST [65–67] and the TeV ACT detectors. More detailed searches and analyses by the experimental collaborations themselves should also lead to improvements, which we encourage. These searches for dark matter signals are already background-limited, which will limit the possible improvements. GLAST and other experiments should be able to make reductions in the backgrounds by taking advantage of better energy and angular resolution, and by reducing the residual diffuse emission by subtracting astrophysical components and resolving individual sources. The high statistics expected for GLAST and other experiments should also make it possible to define detection criteria in terms of the uncertainty on the background, instead of the whole measured background.

Using a conservative choice on the branching ratio to gamma rays, namely $\mathrm{Br}(\gamma\gamma) \simeq 10^{-4}$, we defined an upper limit on the *total* dark matter annihilation cross section by dividing our limits on the partial cross section to gamma rays by this branching ratio. At intermediate energies, the upper limit on the total cross section defined this way is comparable to previous upper limits defined using neutrinos [7,8,29]. The combined limit is considerably stronger than the unitarity bound [24,25], or the cross section of Ref. [4], which would lead to substantial modifications of dark matter halos. For the relatively large cross sections considered here, the dark matter could not be a thermal relic; additional work is needed to push the sensitivity of these and other techniques down to the expected cross section scale for thermal relics.

ACKNOWLEDGMENTS

We thank Brian Baughman, Matt Kistler, Shmuel Nussinov, Sergio Palomares-Ruiz, and Casey Watson for useful discussions and comments. G. D. M. was supported by the Department of Energy Grant No. DE-FG02-91ER40690, T. D. J. by the Commonwealth of Australia, N. F. B. by the University of Melbourne Early Career Researcher and Melbourne Research Grant Schemes, and J. F. B. and H. Y. by NSF CAREER Grant No. PHY-0547102 to J. F. B.

[1] G. Jungman, M. Kamionkowski, and K. Griest, Phys. Rep. **267**, 195 (1996).
[2] G. Bertone, D. Hooper, and J. Silk, Phys. Rep. **405**, 279 (2005).
[3] L. Bergstrom, Rep. Prog. Phys. **63**, 793 (2000).
[4] M. Kaplinghat, L. Knox, and M. S. Turner, Phys. Rev. Lett. **85**, 3335 (2000).
[5] S. Das and N. Weiner, arXiv:astro-ph/0611353.

[6] P. Ullio, L. Bergstrom, J. Edsjo, and C. G. Lacey, Phys. Rev. D **66**, 123502 (2002).
[7] J. F. Beacom, N. F. Bell, and G. D. Mack, Phys. Rev. Lett. **99**, 231301 (2007).
[8] H. Yuksel, S. Horiuchi, J. F. Beacom, and S. Ando, Phys. Rev. D **76**, 123506 (2007).
[9] M. Kachelriess and P. D. Serpico, Phys. Rev. D **76**, 063516 (2007).
[10] N. F. Bell, J. B. Dent, T. D. Jacques, and T. J. Weiler, arXiv:0805.3423.
[11] J. B. Dent, R. J. Scherrer, and T. J. Weiler, Phys. Rev. D **78**, 063509 (2008).
[12] D. Hooper, Phys. Rev. D **77**, 123523 (2008).
[13] A. Bouquet, P. Salati, and J. Silk, Phys. Rev. D **40**, 3168 (1989).
[14] S. Rudaz and F. W. Stecker, Astrophys. J. **368**, 406 (1991).
[15] A. R. Pullen, R. R. Chary, and M. Kamionkowski, Phys. Rev. D **76**, 063006 (2007).
[16] P. D. Serpico and G. Zaharijas, Astropart. Phys. **29**, 380 (2008).
[17] S. Profumo, Phys. Rev. D **78**, 023507 (2008).
[18] M. Cirelli, R. Franceschini, and A. Strumia, Nucl. Phys. **B800**, 204 (2008).
[19] M. Pospelov and A. Ritz, Phys. Rev. D **78**, 055003 (2008).
[20] S. Matsumoto, J. Sato, and Y. Sato, arXiv:hep-ph/0505160.
[21] M. Gustafsson, E. Lundstrom, L. Bergstrom, and J. Edsjo, Phys. Rev. Lett. **99**, 041301 (2007).
[22] F. Ferrer, L. M. Krauss, and S. Profumo, Phys. Rev. D **74**, 115007 (2006).
[23] M. T. Ressell and M. S. Turner, Comments Astrophys. **14**, 323 (1990).
[24] K. Griest and M. Kamionkowski, Phys. Rev. Lett. **64**, 615 (1990).
[25] L. Hui, Phys. Rev. Lett. **86**, 3467 (2001).
[26] A. Kusenko and P. J. Steinhardt, Phys. Rev. Lett. **87**, 141301 (2001).
[27] J. F. Beacom, N. F. Bell, and G. Bertone, Phys. Rev. Lett. **94**, 171301 (2005); L. Bergstrom, T. Bringmann, M. Eriksson, and M. Gustafsson, Phys. Rev. Lett. **94**, 131301 (2005).
[28] D. Fargion, R. Konoplich, M. Grossi, and M. Khlopov, Astropart. Phys. **12**, 307 (2000); E. A. Baltz and L. Wai, Phys. Rev. D **70**, 023512 (2004); D. P. Finkbeiner, arXiv:astro-ph/0409027.
[29] S. Palomares-Ruiz and S. Pascoli, Phys. Rev. D **77**, 025025 (2008).
[30] S. Palomares-Ruiz, Phys. Lett. B **665**, 50 (2008).
[31] J. F. Navarro, C. S. Frenk, and S. D. M. White, Astrophys. J. **462**, 563 (1996).
[32] A. V. Kravtsov, A. A. Klypin, J. S. Bullock, and J. R. Primack, Astrophys. J. **502**, 48 (1998).
[33] M. Fornasa, M. Taoso, and G. Bertone, Phys. Rev. D **76**, 043517 (2007).
[34] N. Fornengo, L. Pieri, and S. Scopel, Phys. Rev. D **70**, 103529 (2004).
[35] J. Diemand, M. Kuhlen, and P. Madau, Astrophys. J. **657**, 262 (2007).
[36] L. E. Strigari, S. M. Koushiappas, J. S. Bullock, M. Kaplinghat, J. D. Simon, M. Geha, and B. Willman, arXiv:0709.1510.
[37] G. Bertone, A. R. Zentner, and J. Silk, Phys. Rev. D **72**, 103517 (2005).
[38] S. Horiuchi and S. Ando, Phys. Rev. D **74**, 103504 (2006).
[39] A. Falvard *et al.*, Astropart. Phys. **20**, 467 (2004).
[40] N. W. Evans, F. Ferrer, and S. Sarkar, Phys. Rev. D **69**, 123501 (2004).
[41] L. Bergstrom, J. Edsjo, and P. Ullio, Phys. Rev. Lett. **87**, 251301 (2001).
[42] NASA CGRO Support Center—COMPTEL experiment, http://cossc.gsfc.nasa.gov/docs/cgro/cgro/comptel.html.
[43] NASA CGRO Support Center—EGRET experiment, http://cossc.gsfc.nasa.gov/docs/cgro/cgro/egret.html.
[44] A. W. Strong, H. Bloemen, R. Diehl, W. Hermsen, and V. Schoenfelder, Astrophys. Lett. Commun. **39**, 209 (1999).
[45] A. W. Strong *et al.*, Astron. Astrophys. **444**, 495 (2005); S. D. Hunter *et al.*, Astrophys. J. **481**, 205 (1997); F. W. Stecker, S. D. Hunter, and D. A. Kniffen, Astropart. Phys. **29**, 25 (2008).
[46] HESS experiment, http://www.mpi-hd.mpg.de/hfm/HESS/HESS.html.
[47] F. Aharonian *et al.* (H.E.S.S. Collaboration), Nature (London) **439**, 695 (2006).
[48] INTEGRAL experiment, http://www.sciops.esa.int/integral.
[49] B. J. Teegarden and K. Watanabe, Astrophys. J. **646**, 965 (2006).
[50] J. F. Beacom and H. Yuksel, Phys. Rev. Lett. **97**, 071102 (2006).
[51] R. Diehl *et al.*, Nature (London) **439**, 45 (2006).
[52] H. Yuksel, J. F. Beacom, and C. R. Watson, arXiv:0706.4084 [Phys. Rev. Lett. (to be published)].
[53] J. J. Blom, T. A. D. Paglione, and A. Carraminana, arXiv:astro-ph/9811389.
[54] CELESTE experiment, http://doc.in2p3.fr/themis/CELESTE/.
[55] J. Lavalle *et al.*, Astron. Astrophys. **450**, 1 (2006).
[56] HEGRA experiment, http://www-hegra.desy.de/.
[57] F. A. Aharonian *et al.* (HEGRA Collaboration), Astron. Astrophys. **400**, 153 (2003).
[58] E. Churazov *et al.*, Astron. Astrophys. **467**, 529 (2007).
[59] G. Weidenspointner *et al.*, AIP Conf. Proc. **510**, 467 (2000).
[60] A. W. Strong, I. V. Moskalenko, and O. Reimer, Astrophys. J. **613**, 956 (2004).
[61] NASA HEASARC—SMM experiment, http://heasarc.nasa.gov/docs/heasarc/missions/solarmax.html.
[62] K. Watanabe, M. D. Leising, G. H. Share, and R. L. Kinzer, AIP Conf. Proc. **510**, 471 (2000).
[63] H. Yuksel and M. D. Kistler, Phys. Rev. D **78**, 023502 (2008).
[64] S. Profumo, Phys. Rev. D **77**, 103510 (2008).
[65] A. Morselli, Nucl. Phys. B, Proc. Suppl. **134**, 127 (2004); AIP Conf. Proc. **745**, 422 (2005).
[66] A. Morselli, Chin. J. Astron. Astrophys. **6**, Suppl-1, 349 (2006).
[67] E. A. Baltz *et al.*, J. Cosmol. Astropart. Phys. 07 (2008) 013.